Analysis of melting and solidification processes in the phase-change device of an energy storage interconnected heat pump system

Cite as: AIP Advances **10**, 055021 (2020); https://doi.org/10.1063/5.0006280
Submitted: 01 March 2020 • Accepted: 03 May 2020 • Published Online: 19 May 2020

Xiang Gao, Wenke Zhang, Zhaohong Fang, et al.

Analysis of melting and solidification processes in the phase-change device of an energy storage interconnected heat pump system

Cite as: AIP Advances 10, 055021 (2020); doi: 10.1063/5.0006280
Submitted: 1 March 2020 • Accepted: 3 May 2020 •
Published Online: 19 May 2020

Xiang Gao,[1] Wenke Zhang,[1,a)] Zhaohong Fang,[2] Xing Hou,[1] and Xin Zhang[1]

AFFILIATIONS

[1]School of Thermal Engineering, Shandong Jianzhu University, Jinan 250101, People's Republic of China
[2]Shandong Zhongrui New Energy Technology Co., Ltd., Jinan 250000, People's Republic of China

[a)]**Author to whom correspondence should be addressed:** wenkezhang2006@163.com. **Telephone:** +86 0531 86367629. **Fax:** +86 0531 86361236

ABSTRACT

In this paper, an energy storage interconnected heat pump system is proposed. Numerical simulation is performed to investigate the melting and solidification processes of paraffin in a spherical heat storage unit. The influences of the spherical wall temperature, spherical heat storage unit size, and initial temperature of the phase-change material during the melting process, as well as the influence of the spherical wall temperature on the solidification process, were analyzed. The results indicated that the size of the spherical heat storage unit had the most dominant influence on the melting and solidification processes. The overall melting time was less than the overall solidification time at the same temperature difference. In the melting process, convective heat transfer invariably occurs between the liquid phase and the spherical wall, which accelerates the melting process.

NOMENCLATURE

a	diffusion coefficient (k/c)
COP	coefficient of performance
g	gravitational acceleration
h	enthalpy (kJ/kg)
h_{ext}	the convective heat transfer coefficient (W m^{-2} K^{-1})
P	pressure (Pa)
PCM	phase change material
T	temperature (K)
T_{ext}	the temperature of the external heat transfer fluid (K)
T_i	the initial temperature of the PCM (K)
T_l	the temperature of the liquid (K)
Ts	the temperature of the solid (K)
u	the velocities along the x directions
$\vec{V}$	the velocity vector
$\vec{V}_l$	the velocity vector of the liquid PCM
$\vec{V}_s$	the velocity vector of the solid PCM
v	the velocities along the y directions
μ	N s/m^2
ρ	density (kg m^{-3})
τ	time (s)

I. INTRODUCTION

In different energy utilization and conversion systems, the heat storage and release characteristics of a heat storage device can be used to solve the contradiction between supply and demand in terms of time and space because heat storage devices are widely used in solar energy storage systems,[1–3] solar power systems,[4–6] and industrial heating and cooling air conditioning systems.[7–11] A new type of energy storage interconnected heat pump system for low-temperature regions is analyzed in this study. Figure 1 shows that two phase-change thermal energy storage devices can be employed to connect the air source heat pump on the low-temperature side with the water source heat pump on the high-temperature side, with paraffin acting as the phase-change material (PCM). Water at 15 °C is produced by the air source heat pump. Then, this water exchanges

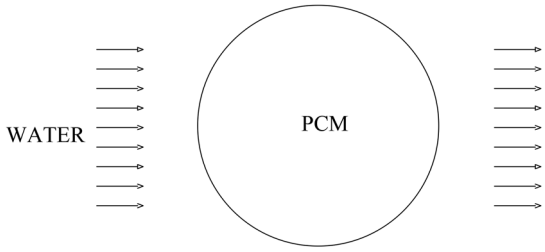

FIG. 1. Structure of the spherical heat storage unit.

heat with the phase-change heat storage system. The water at the source heat pump absorbs heat from this energy storage system and supplies water at 50 °C to the end equipment. For the energy storage interconnected heat pump system, it is favorable to reduce the compression ratio with the aid of both the low condensation temperature of the air source heat pump and the high evaporation temperature of the water source heat pump. A spherical heat storage unit is used in the heat storage device, and spheres filled with the PCM are deposited inside a tank in which water bathes the spheres.

For such a spherical heat storage unit, numerical simulations were performed for two spherical erythritol-filled units having different diameters.[12] In the simulation, the external convection process of the sphere, heat conduction of the wall of the sphere, natural convection of the liquid phase inside the sphere, volume expansion of the PCM during melting, and motion of the solid phase during melting were considered to influence the melting process. The results indicated that the main factors affecting the melting process were differences in the heat transfer temperature between the inside and the outside of the sphere, Reynolds number of the external heat transfer fluid, and position of the spheres in the tank. The solidification process in four spherical units having different diameters (10 mm, 20 mm, 30 mm, and 40 mm) was investigated using experimental and numerical methods,[13] and the results indicated that the effects of the sphere diameter during solidification were stronger than the effects of temperature differences under different initial conditions with a varying set of initial temperatures. As such, a standard verification model of the solidification process was proposed. Several scholars have analyzed the constrained melting process in a paraffin-filled spherical heat storage unit,[14,15] and the results have indicated that small units in the tank help to improve the heat storage performance of the overall unit, while the thermal conductivity of the shell has little effect on the heat storage process. Unconstrained melting in a spherical unit was studied using n-octadecane as the PCM. A combination of experimental and numerical methods was used to calculate the Grashof, Stefan, and Fourier numbers of the unconstrained phase-transition process. The results showed that heat conduction was the dominant mode of heat transfer during the initial stages of melting. As the melting process continued, the effect of natural convention was enhanced. In a simulation process with three different shell diameters (40 mm, 60 mm, and 80 mm), changes in wall temperature had a stronger effect on the heat storage process of a small-sized spherical heat storage unit.[16] Numerical analysis of spherical heat storage units having different diameters yielded the same result.[17] Unconstrained melting of paraffin in a sphere was visualized, and the melting process of paraffin was recorded using a digital camera.[18] The results indicated a correlation between *Fo*, *Ra*, *Ste*, S_t, ε, and melting time.

In this type of spherical heat storage system, air is mostly used as an external heat transfer fluid to complete the heat transfer process of the PCM. Experts have investigated the volumetric heat transfer coefficient between spherical heat storage units and water.[19] The wall of the spherical unit was made of steel (SS304). The final result indicated that the volumetric heat transfer coefficient can be corrected to obtain an experimental formula for using water as the external heat transfer fluid. Researchers investigated the melting and solidification processes of paraffin, a low-temperature PCM, by using experimental and numerical methods.[20] The diameter of the spherical heat storage unit used in this analysis was 40 mm, and spheres filled with the PCM were deposited inside a 0.25 × 0.25 m^2 square tank in which air flowed through the spheres. In the square tank, air acted as an external heat transfer fluid that exchanged heat with the heat storage unit. The results showed that a dimensionless relationship between the melting and solidification processes could be obtained.

This work reveals the melting process that occurs in pebble bed heat storage units containing spheres through an external convective heat transfer process, heat conduction through the sphere wall, natural convection of the liquid phase, volume expansion or contraction of the PCMs during the melting and solidification processes, and movement of the solid phase during the melting or solidification process. We analyze a spherical heat storage unit that uses paraffin as a low-temperature PCM and investigate the melting and solidification processes that occur in a spherical heat storage unit.

II. ESTABLISHMENT OF MATHEMATICAL MODELS

A. Physical description of a phase-change device

Figure 1 describes the structure of a phase-change heat storage device. The heat exchange fluid (water) flows into the device and passes through the spherical heat storage unit located in the phase-change device for heat transfer. Then, water flows out of the device. The spherical heat storage unit is filled with paraffin C17. In order to simplify the model, it is assumed that there is no contact between the spherical phase change units and the spherical wall has enough elasticity without failure when the volume of the phase change material expands. Then, the numerical simulation analyzes the spherical phase change unit size, spherical wall temperature, and initial temperature of the phase change material on the idealized model. The properties of the PCM are summarized in Table I.

TABLE I. Thermal and physical properties of paraffin C17.

Characteristic	Value (material: C17)
Density (g/m^3)	789 liquid 900 solid
Latent heat (kJ/kg)	171.5
Thermal conductivity [w/(m J)]	0.21
Specific heat [J/(kg K)]	2 100
Viscosity [Pa s]	0.006 89

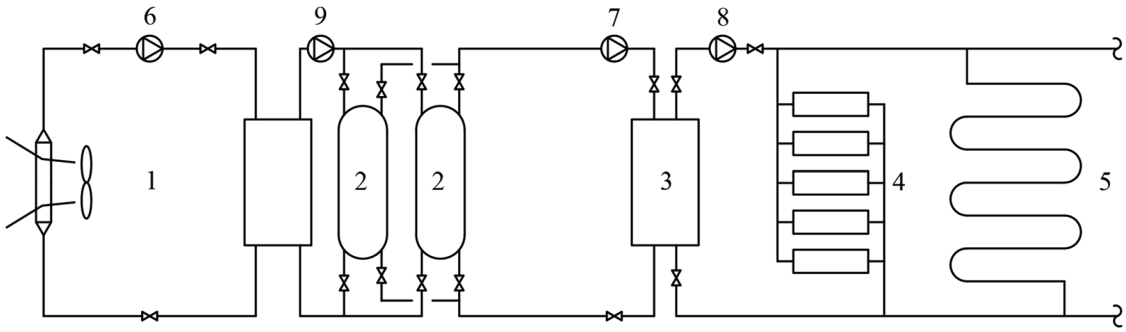

FIG. 2. Schematic diagram of the energy storage interconnected heat pump system. (1) Air source heat pump, (2) phase-change energy storage device, (3) water source heat pump, [(4) and (5)] users, and [(6)–(9)] water pump.

B. Formulas used to calculate properties of energy storage interconnected heat pump

Heat is extracted from air by means of a low-temperature air source heat pump. Subsequently, heat exchange occurs in the phase-change heat storage device, which means heat is stored in the PCM. Thereafter, the phase-change heat storage device releases heat to the water loop of the water source heat pump, and thus, heating for buildings is achieved. A phase-change energy storage device was employed to connect the air source and water source heat pumps. Figure 2 shows a schematic diagram of the system structure.

C. Phase-change heat storage device model

1. Model description

A structural model of the phase-change heat storage device is shown in Fig. 3. The external heat transfer fluid water flows in from one end of the phase-change device and then exchanges heat with the phase-change heat storage unit. Finally, numerical simulations of the phase-change unit in the device were performed.

The phase-change heat storage unit was designed with a spherical structure. Spheres filled with the PCM were deposited inside a tank in which they were bathed in external water. The effects of sphere wall thickness on the solidification and melting processes were not considered in this simulation.

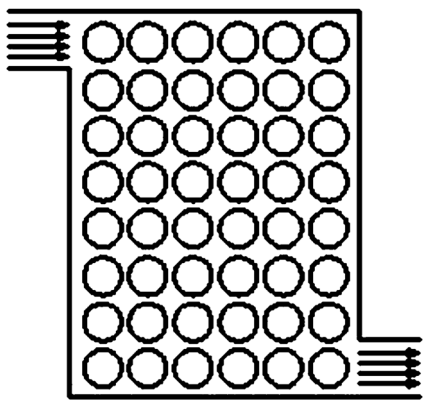

FIG. 3. Structure of the phase-change heat storage device.

The mathematical model used to solve the problem consisted of the conservation of mass, momentum, and energy equations, as well as an enthalpy–porosity model adapted from an existing model.[21] The enthalpy–porosity model employed only enthalpy and temperature as the dependent variables to solve the problem without tracking the two-phase interface. An unsteady, laminar, and incompressible flow was assumed. The mass conservation is expressed as follows:

$$\frac{\partial \rho}{\partial t} + \mathrm{div}\left(\rho \vec{V}\right) = 0, \tag{1}$$

where $\vec{V}$ is the velocity, ρ is the density, and t is the time. This simulation process considers natural convection of the liquid phase during solidification of the PCM. Thus, it was necessary to include a natural convection term in the dynamic equation. The momentum equation is given as follows:

$$\frac{\partial(\rho u)}{\partial t} + \mathrm{div}\left(\rho \vec{V} u\right) = \mathrm{div}(\mu grad u) - \frac{\partial P}{\partial x} + S_u, \tag{2}$$

$$\frac{\partial(\rho v)}{\partial t} + \mathrm{div}\left(\rho \vec{V} v\right) = \mathrm{div}(\mu grad v) - \frac{\partial P}{\partial y} + \rho g + S_v, \tag{3}$$

where u and v are the velocities along the x and y directions, respectively, P is the pressure, g is the gravitational acceleration, and μ is the dynamic viscosity. S_u and S_v are expressed as follows:

$$S_u = -C\frac{(1-\varepsilon)^2}{\varepsilon^3 + b}u, \tag{4}$$

$$S_v = -C\frac{(1-\varepsilon)^2}{\varepsilon^3 + b}v, \tag{5}$$

where C is the mushy zone constant, ε is the liquid volume fraction, and b is a constant with a small value of 0.001 to prevent the source term denominator from becoming equal to 0. ε is given as follows:

$$\varepsilon = 0, \quad T < T_s, \tag{6}$$

$$\varepsilon = 1, \quad T > T_l, \tag{7}$$

$$\varepsilon = \frac{T - T_s}{T_l - T_s}, \quad T_s < T < T_l, \tag{8}$$

where T is the temperature, T_s is the solid phase temperature, and T_l is the liquid phase temperature. The energy equation is given as follows:

$$\frac{\partial(\rho h)}{\partial t} + \mathrm{div}\left(\rho \vec{V} h\right) = \mathrm{div}(\alpha gradh), \tag{9}$$

where a is the diffusion coefficient (k/c) and h is enthalpy, which is expressed as follows:

$$h = \int_{T_{ref}}^{T} cdT. \tag{10}$$

2. Initial and boundary conditions

The initial temperature of the thermal storage unit shell was set to be equal to the initial temperature of the external heat exchange fluid (water). The interior of the shell was described using a non-slip boundary condition. The initial and boundary conditions are expressed as follows:

$$T_s|t = 0 = T_i, \tag{11}$$

$$\vec{V}_s|t = 0 = 0, \tag{12}$$

$$-k\frac{\partial T}{\partial \tau}\Big|_{y=l}^{x=l} = h_{ext}(T_L - T_{ext}), \tag{13}$$

$$\vec{V}_s\Big|_{y=l}^{x=l} = 0, \tag{14}$$

where T_i is the initial temperature of the PCM, T_l is the temperature of the liquid, $\vec{V}_l$ is the velocity vector of the liquid PCM, $\vec{V}_s$ is the velocity vector of the solid PCM, h_{ext} is the convective heat transfer coefficient, and T_{ext} is the temperature of the external heat transfer fluid.

D. Simulation for control

The convergence criteria in all cases were set as follows: 10^{-8} for the energy equation and 10^{-6} for the momentum and mass conservation equation. The under-relaxation factors were set as 0.3 for pressure, 0.2 for the liquid fraction, 0.9 for energy, 0.5 for field forces, 0.4 for momentum, and 0.6 for density. The pressure–velocity coupling was performed using the PSIO method while the PRESTO scheme was used for pressure correction. A second-order upwind scheme was utilized to solve the momentum and energy equations. A geo-reconstruct method was employed to correct the liquid fraction in the volume of fluid model. The calculations considered the effects of natural convection on the solidification process. Finally, the results compared the liquid fraction of the PCM inside the phase-change heat storage unit.

E. Grid analysis and model verification

To reduce simulation time, grids comprising 8500, 10 500, and 13 200 meshes were tested. The simulation settings were as follows: a spherical wall temperature of 7 °C and the most unstable time step (0.2 s) were used to test the meshes. The variations in the liquid fraction β obtained with the three tested grids are shown in Fig. 4. The trend of the solidification process is roughly consistent with the trend of changes in the liquid fraction, as described in the literature. Finally, the grid consisting of 10 500 meshes was selected.

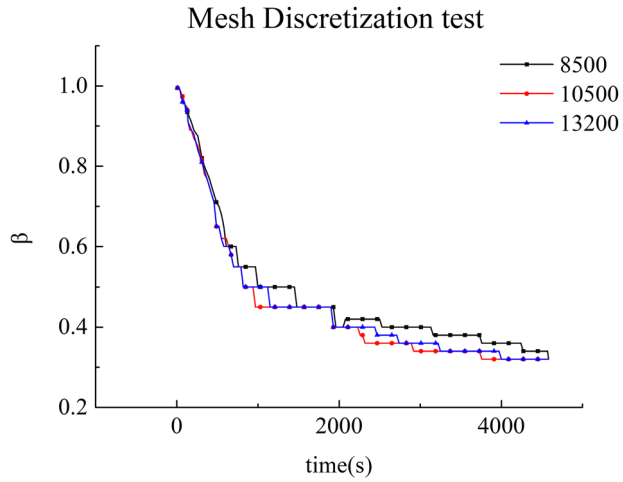

FIG. 4. Grid-independent verification.

Time steps of 0.1 s, 0.3 s, and 0.6 s were tested, and the divergence problem was found to occur at 0.3 s. The settings were the same as above (water temperature of 7 °C). As shown in Fig. 5, considering the time saved in calculation, a step size of 0.1 s was employed in the simulations after several testing steps. The mushy zone constant C = 2.0×10^4, as in Eqs. (4) and (5), was used in the simulation.

III. RESULTS AND ANALYSIS

A. Influence of spherical heat storage unit size on melting process

The influence of the spherical heat storage unit size on the melting process was numerically simulated. The diameter of the spherical

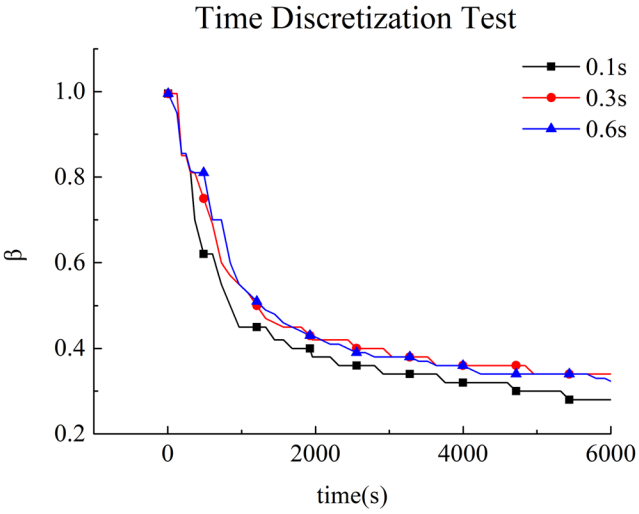

FIG. 5. Liquid volume fraction curve for different time step sizes.

unit was set to 10 mm, 20 mm, 30 mm, and 40 mm in the simulation. The wall temperature and the initial PCM temperature were set to 28 °C and 17 °C, respectively. The liquid volume fractions of the spherical units are shown in Fig. 6.

The complete melting times (β = 1) for the four spherical heat storage units increased as the diameter of the unit increased. When the diameter of the unit was 40 mm, the complete melting time increased by 2.8 times compared to that when the diameter of the unit was 30 mm. When the diameter was 20 mm, the complete melting time increased by 1.7 times compared to that when the diameter was 10 mm. Therefore, in terms of only the internal melting process of the spherical heat storage unit, selection of a unit with a small diameter significantly reduced the melting time and improved the heat storage performance of the phase-change heat storage device. The complete melting time for the unit with the diameter of 40 mm was significantly longer than those of the other units, mainly owing to the requirement of a larger quantity of PCMs contained in the unit.

According to Fig. 6, the liquid volume fraction varies greatly between 40 mm and 10 mm diameters. In order to accurately analyze the effort of volume on the melting process, the diameter of the spherical unit was set to 10 mm, 12.6 mm, 14.4 mm, and 15.9 mm in the simulation. The volume of 12.6 mm, 14.4 mm, and 15.9 mm is twice, three times, and four times of 10 mm, respectively. The liquid volume fractions of the spherical units are shown in Fig. 7. The simulation results show that the complete melting times of 12.6 mm, 14.4 mm, and 15.9 mm is 1.1 times, 1.3 times, and 1.4 times of 10 mm, respectively. The external heat area of 12.6 mm, 14.4 mm, and 15.9 mm is 1.59 times, 2.07 times, and 2.52 times of 10 mm, respectively. Comparing the complete melting time of volume and external heat area on the melting process, the impact of the external heat area is more significant than the volume in the spherical phase change unit.

B. Influence of wall temperature on melting process

According to the operating conditions of the energy storage interconnected heat pump system, three wall temperatures of 23 °C, 25 °C, and 28 °C were employed in the simulation. The initial temperature of the PCM was set to 17 °C. The diameter of the spherical unit was set to 20 mm. As shown in Fig. 8, the complete melting time for the PCM decreased as the wall temperature increased. When the wall temperature was 28 °C, the complete melting time was 3000 s, which is about twice as long as that at 23 °C and 1.3 times as long as that at 25 °C.

The effect of changing the wall temperature was found to be weaker than that of changing the unit size for wall temperatures of 20–30 °C. For spherical phase-change units, changes in the size of the unit (i.e., changes in the quantity of the PCM) significantly influence the total melting time.

C. Influence of initial temperature on melting process

Another factor that affects the melting process is the initial PCM temperature. Initial PCM temperatures of 12 °C, 14 °C, and 17 °C were employed in the simulation. The final results are shown in Fig. 9.

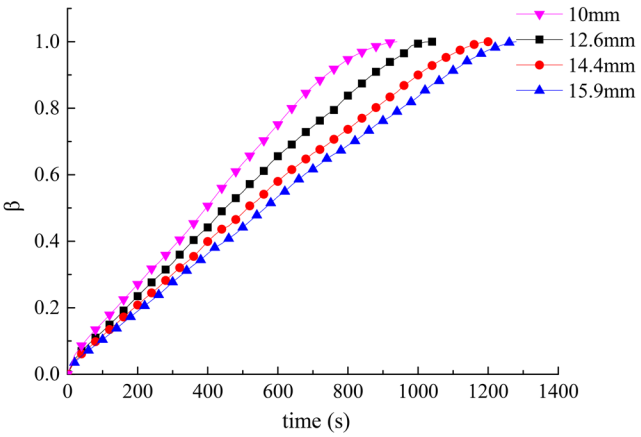

FIG. 7. Liquid volume fraction curves at different diameters.

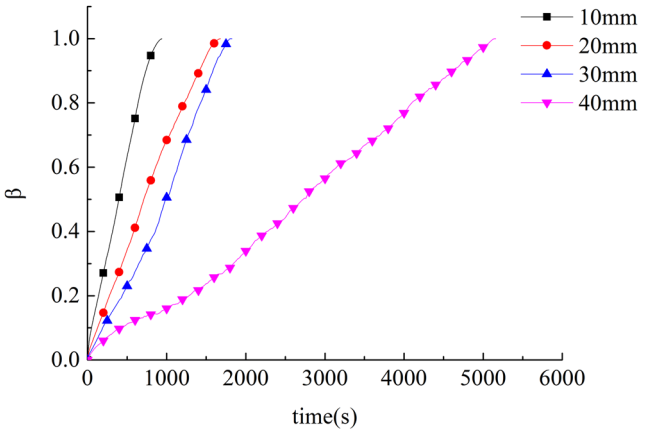

FIG. 6. Liquid volume fraction curves of different heat storage units.

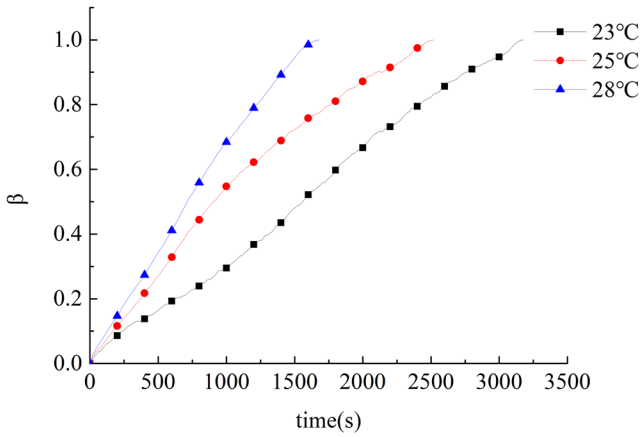

FIG. 8. Liquid volume fraction curves at different wall temperatures.

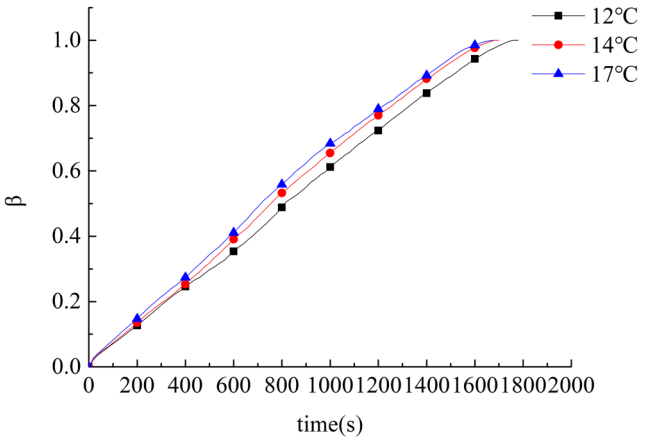

FIG. 9. Liquid volume fraction curves at different initial temperatures.

When the initial temperature is lower, the complete melting time of paraffin was longer. A difference of only 5% in the complete melting time of the PCM was observed between initial PCM temperatures of 12 °C and 17 °C. Therefore, for several common initial temperatures of the spherical phase-change unit in this system, changes in the initial temperature had no significant impact on the thermal storage performance of the phase-change spheres, and the initial PCM temperature has the weakest effect on the melting process.

D. Influence of wall temperature on melting process

As shown in Figs. 10(a) and 10(b), from the perspective of the water loop temperature on both sides of the phase-change heat storage device, the coefficient of performance (COP) of the low-temperature-side air source heat pump decreases as the inlet temperature of the phase-change device decreases during the melting process when the outdoor temperature is −20 °C and the terminal water supply temperature is 50 °C. The COP of the high-temperature-side water source heat pump increases as the inlet temperature of the phase-change device increases during the solidification process. Thus, it is necessary to select a higher inlet temperature for the phase-change device during the melting process and a higher outlet temperature for the phase-change device during the solidification process when setting the water loop temperature on both sides of the heat storage device.

In the simulation process, the phase-transition temperature of paraffin was 20 °C, and the volume fractions of the PCM liquid during the solidification process in the phase-change heat storage device were compared assuming the following three conditions: (1) an inlet temperature of 17 °C and an outlet temperature of 19 °C, (2) an inlet temperature of 12 °C and an outlet temperature of 15 °C, and (3) an inlet temperature of 7 °C and an outlet temperature of 12 °C. Considering natural convection, the wall temperature boundary conditions were simplified to 7 °C, 12 °C, and 17 °C. As shown in Fig. 11, the liquid fraction of the PCM changed at 7 °C, 12 °C, and 17 °C.

Figure 11 shows that the times required for the complete solidification of paraffin C17 are 4.2 h, 4.8 h, and 6.9 h when the phase-change energy storage unit is bathed in water at 7 °C, 12 °C, and

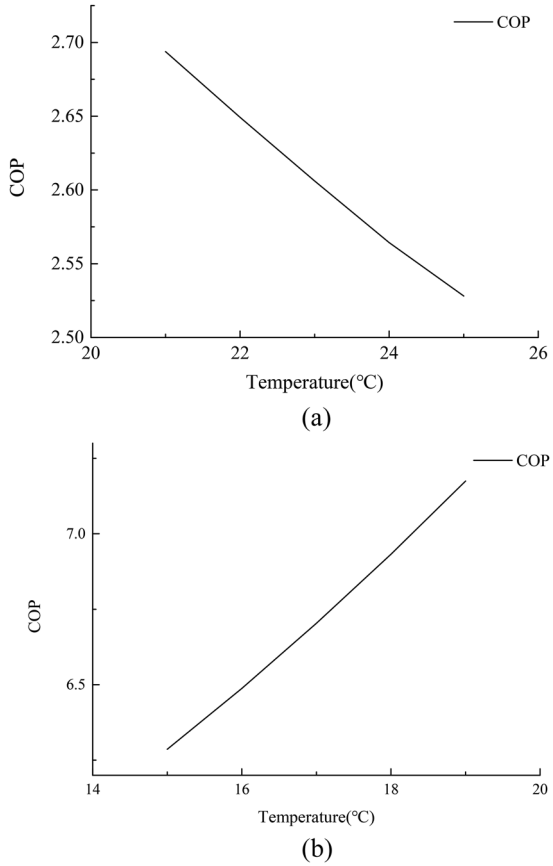

FIG. 10. Changes in COP with different inlet temperatures for phase-change devices. (a) Changes in COP of low-temperature side at different inlet temperatures during heat storage. (b) Changes in COP of high-temperature side at different outlet temperatures during the exothermic process.

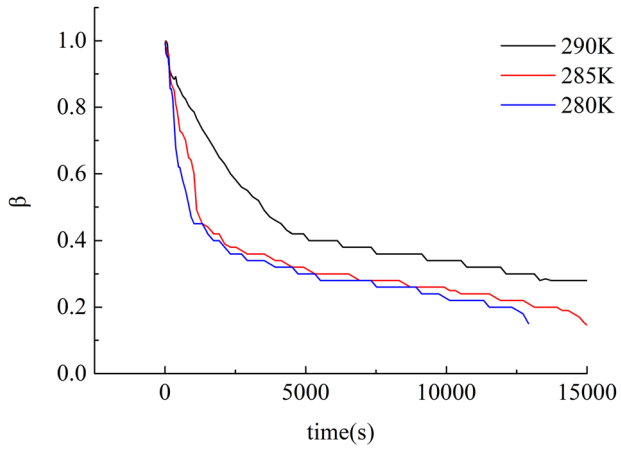

FIG. 11. Liquid fraction curve of the phase-change material.

17 °C, respectively. The complete solidification times of the PCM are approximately equal for the water temperatures of 7 °C and 12 °C. Thus, the selection of a higher inlet temperature for the high-temperature water source heat pump will lead to an increase in COP. Therefore, for maximizing device efficiency, the phase-change device should be designed with a water inlet temperature of 12 °C.

There are two heat transfer stages in the solidification process in the spherical heat storage device. In the initial solidification process,

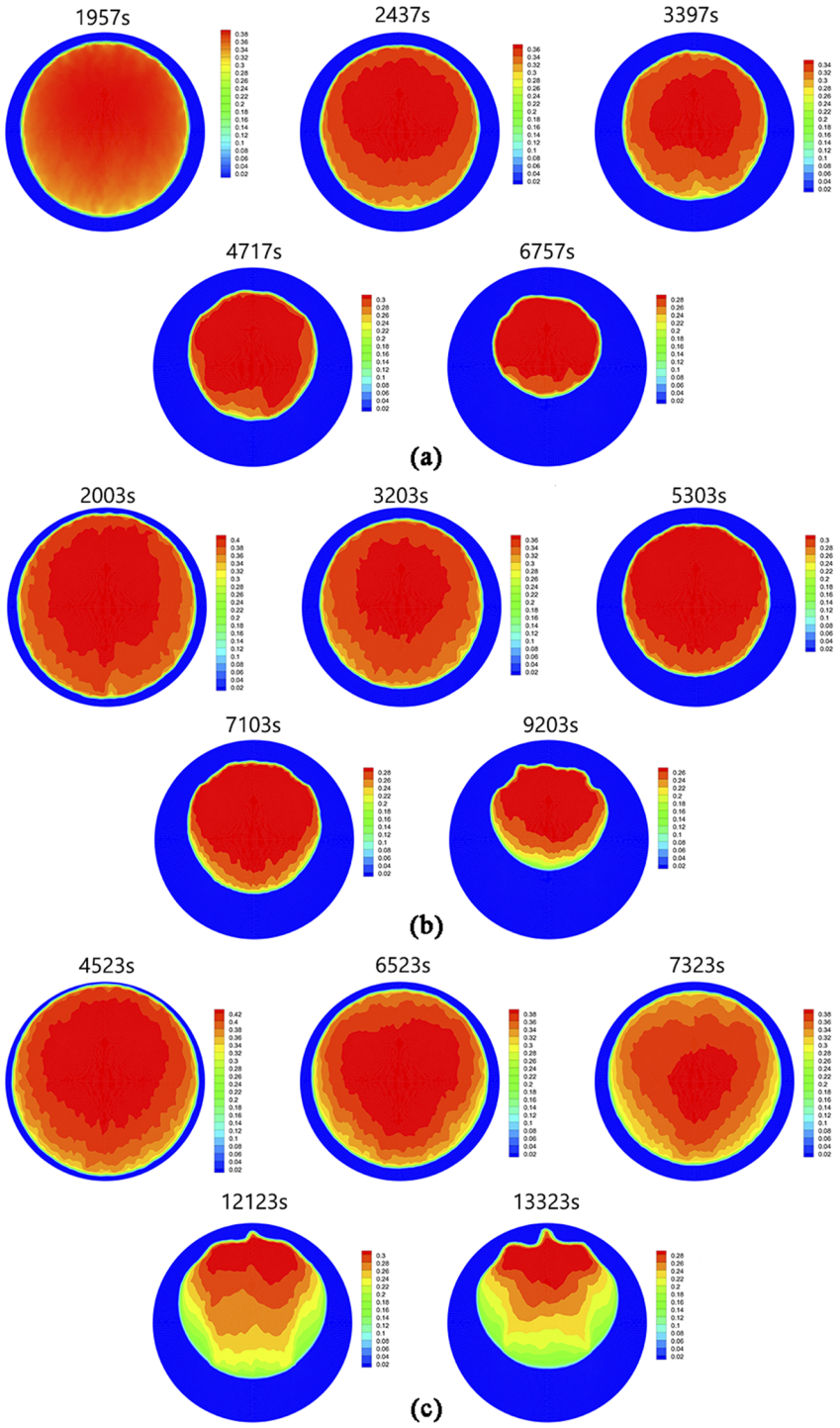

FIG. 12. Variations in liquid volume fraction of phase change materials at different wall temperatures: (a) 7 °C, (b) 12 °C, and (c) 17 °C.

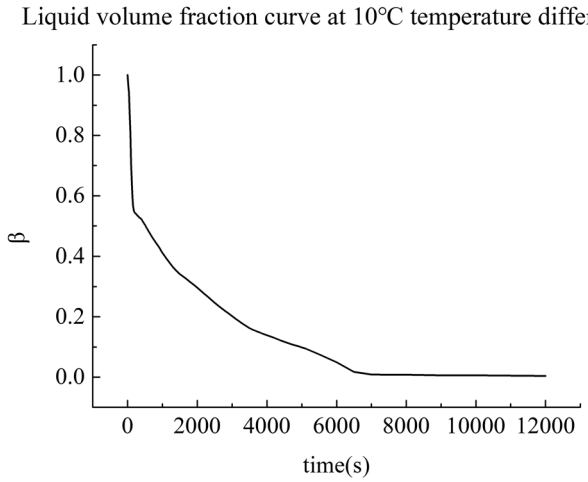

FIG. 13. Liquid fraction curve of the PCM with a 10 °C difference during the solidification process.

the PCM is in a liquid state, and natural convection is the main heat transfer process. In this stage, the solidification rate of the PCM is the highest. As the solidification process progresses, heat conduction gradually influences the solidification process as the main heat transfer process. Figure 12 shows PCM solidification at different liquid fractions.

There are two main stages of heat transfer in the solidification process in a ball-type heat storage device. At the start of solidification, the PCM is in a liquid state. At this time, natural convection is the main mode of heat transfer, and the PCM solidification rate is the highest. As the solidification process progresses, the proportion of the solid PCM increases, natural convection process gradually weakens, and heat conduction gradually becomes the main mode of heat transfer in the solidification process.

Because organic PCMs have low thermal conductivity, when natural convection is no longer the dominant mode of heat transfer, the entire solidification process slows down. Low thermal conductivity is not conducive for the exothermic process occurring in the unit. As shown in Fig. 13, the complete melting and solidification times of the two processes at the temperature difference of 10 °C between the initial and the wall temperatures are compared. During the melting process, liquid-phase materials are continuously generated, and they cover the surface of the solid-phase materials. Convective heat transfer between the spherical wall and the liquid PCMs always exists in the melting stage, and it improves the melting rate. Therefore, the complete melting time of paraffin is less than its complete solidification time.

IV. CONCLUSIONS

In this paper, the melting and solidification processes of a phase-change unit filled with paraffin C17 were investigated through numerical simulations. The numerical model incorporates the following: spherical heat storage unit size, wall temperature, and initial temperature. The complete melting and solidification times were investigated by means of comparison with the melting and solidification results available in simulations. The main results are summarized as follows:

(1) In the melting process in a spherical phase-change unit, the main factors affecting the melting rate are as follows: the size of the phase-change spherical unit, wall temperature, and initial PCM temperature. The factors with the strongest and the weakest effects are the size of the phase-change spherical unit and initial PCM temperature, respectively.
(2) During the solidification process in the spherical phase-change unit, an increase in the quantity of the solid-phase material reduced convective heat transfer between the liquid phase and the spherical wall, thus reducing the solidification rate.
(3) The complete melting time was less than the complete solidification time when the spherical heat storage unit was filled with paraffin. In the melting process, convective heat transfer invariably occurs between the liquid phase and the spherical wall, which accelerates the melting process.

ACKNOWLEDGMENTS

This work was supported by National Natural Science Foundation of China (Project No. 51708336).

DATA AVAILABILITY

The data that support the findings of this study are available from the corresponding author upon reasonable request.

REFERENCES

[1] M. E. Zayed, J. Zhao, A. H. Elsheikh, F. A. Hammad, L. Ma, Y. Du, A. E. Kabeel, and S. M. Shalaby, "Applications of cascaded phase change materials in solar water collector storage tanks: A review," Sol. Energy Mater. Sol. Cells **199**, 24–49 (2019).
[2] Z. Han, C. Bai, X. Ma, B. Li, and H. Hu, "Study on the performance of solar-assisted transcritical CO_2 heat pump system with phase change energy storage suitable for rural houses," Sol. Energy **174**, 45–54 (2018).
[3] M. Faegh and M. B. Shafii, "Experimental investigation of a solar still equipped with an external heat storage system using phase change materials and heat pipes," Desalination **409**, 128–135 (2017).
[4] K. Bhagat and S. K. Saha, "Numerical analysis of latent heat thermal energy storage using encapsulated phase change material for solar thermal power plant," Renewable Energy **95**, 323–336 (2016).
[5] R. Yogev and A. Kribus, "Operation strategies and performance of solar thermal power plants operating from PCM storage," Sol. Energy **95**, 170–180 (2013).
[6] L. Yang, X. Zhang, and G. Xu, "Thermal performance of a solar storage packed bed using spherical capsules filled with PCM having different melting points," Energy Build. **68**, 639–646 (2014).
[7] K. E. Elfeky, X. Li, N. Ahmed, L. Lu, and Q. Wang, "Optimization of thermal performance in thermocline tank thermal energy storage system with the multilayered PCM(s) for CSP tower plants," Appl. Energy **243**, 175–190 (2019).
[8] G. Peiró, J. Gasia, L. Miró, and L. F. Cabeza, "Experimental evaluation at pilot plant scale of multiple PCMs (cascaded) vs. single PCM configuration for thermal energy storage," Renewable Energy **83**, 729–736 (2015).
[9] G. Mazzucco, G. Xotta, V. A. Salomoni, M. Giannuzzi, and C. E. Maiorana, "Solid thermal storage with PCM materials. Numerical investigations," Appl. Therm. Eng. **124**, 545–559 (2017).
[10] D. Li, J. Wang, Y. Ding, H. Yao, and Y. Huang, "Dynamic thermal management for industrial waste heat recovery based on phase change material thermal storage," Appl. Energy **236**, 1168–1182 (2019).

[11] A. Maccarini, G. Hultmark, N. C. Bergsøe, and A. Afshari, "Free cooling potential of a PCM-based heat exchanger coupled with a novel HVAC system for simultaneous heating and cooling of buildings," Sustainable Cities Soc. **42**, 384–395 (2018).
[12] J. F. R. Junior, R. De Césaro Oliveski, L. A. Oliveira Rocha, and C. Biserni, "Numerical investigation on phase change materials (PCM): The melting process of erythritol in spheres under different thermal conditions," Int. J. Mech. Sci. **148**, 20–30 (2018).
[13] J. H. Nazzi Ehms, R. De Césaro Oliveski, L. A. Oliveira Rocha, and C. Biserni, "Theoretical and numerical analysis on phase change materials (PCM): A case study of the solidification process of erythritol in spheres," Int. J. Heat Mass Transfer **119**, 523–532 (2018).
[14] W. Li, S.-G. Li, S. Guan, Y. Wang, X. Zhang, and X. Liu, "Numerical study on melt fraction during melting of phase change material inside a sphere," Int. J. Hydrogen Energy **42**, 18232–18239 (2017).
[15] Z. Gao, Y. Yao, and H. Wu, "Validation of a melting fraction-based effective thermal conductivity correlation for prediction of melting phase change inside a sphere," Int. J. Therm. Sci. **142**, 247–257 (2019).
[16] S. F. Hosseinizadeh, A. A. Rabienataj Darzi, F. L. Tan, and J. M. Khodadadi, "Unconstrained melting inside a sphere," Int. J. Therm. Sci. **63**, 55–64 (2013).
[17] H. Sattari, A. Mohebbi, M. M. Afsahi, and A. Azimi Yancheshme, "CFD simulation of melting process of phase change materials (PCMs) in a spherical capsule," Int. J. Refrig. **73**, 209–218 (2017).
[18] Z. Gao, Y. Yao, and H. Wu, "A visualization study on the unconstrained melting of paraffin in spherical container," Appl. Therm. Eng. **155**, 428–436 (2019).
[19] S. S. Halkarni, A. Sridharan, and S. V. Prabhu, "Estimation of volumetric heat transfer coefficient in randomly packed beds of uniform sized spheres with water as working medium," Int. J. Therm. Sci. **110**, 340–355 (2016).
[20] S. Loem, T. Deethayat, A. Asanakham, and T. Kiatsiriroat, "Thermal characteristics on melting/solidification of low temperature PCM balls packed bed with air charging/discharging," Case Stud. Therm. Eng. **14**, 100431 (2019).
[21] A. D. Brent, V. R. Voller, and K. J. Reid, "Enthalpy-porosity technique for modeling convection-diffusion phase change: Application to the melting of a pure metal," Numer. Heat Transfer **13**, 297–318 (1988).